Comparing Quantum and Semi-Classical Approaches to Non-Collinear Magnetism in an Electron-Spin Dimer

LUND
UNIVERSITY

Sherwan Jamo Abdi

Supervisor: Claudio Verdozzi

Co-Supervisor: Emil Östberg

Department of Mathematical Physics
Lund University

This dissertation is submitted for the degree of
Bachelor of Science (15 HP)
August 2023

I would like to dedicate this thesis to my family and friends whose support and encouragement have been my source of motivation throughout my educational journey.

Acknowledgements

I would like to acknowledge the support and assistance that I have received from my supervisors. I am grateful to Claudio Verdozzi for giving me the opportunity to study a very interesting topic and for his guidance throughout the project. I would also like to thank Emil Östberg for his valuable assistance and expertise, which was of great benefit to me.

Abstract

In this bachelor thesis, an explorative theoretical analysis is presented on a model system characterized by various and competing magnetic interactions. The system comprises two localized magnetic moments (spins), and a single itinerant electron that hops between two orbitals located at the spins' positions. The spins, treated as either fully quantum, hybrid quantum-classical, or fully classical, interact via Heisenberg exchange and Dzyaloshinskii-Moriya interaction (DMI), with the always quantum-mechanically treated itinerant electron coupled to the spins through s-d (Kondo-like) coupling. The core objective of this research was to scrutinize and compare the results obtained from these three distinct approaches for treating the spins. Findings suggest that the agreement between the different methods improves when the DMI term is less influential than the others, and that slow perturbations tend to enhance the agreement between the solutions. It was observed that the hybrid quantum-classical solutions often align more closely with the full quantum solution than the fully classical ones, with discrepancies arising likely due to complex quantum effects and entanglement. Future research could further this study of the simple model studied here (and related ones) via an extensive exploration in the parameter space, and discern the general conditions under which the mixed quantum-classical methods perform optimally. This in turn would give useful indications on the scope of mixed quantum classical treatments of realistic magnetic materials thereby offering deeper insights into the behavior of such systems.

Table of contents

Nomenclature

Acronyms / Abbreviations

DMI	Dzyaloshinskii–Moriya interaction
HE	Heisenberg exchange
LLG	Landau-Lifshitz-Gilbert

Chapter 1

Introduction

Magnetism plays a significant role in shaping modern society, providing the basis for many technological advancements such as superconductors, communication technologies, and data storage [1]. Over the past twenty years, the discovery of a novel magnetic quasi-particle, referred to as a magnetic skyrmion, has stirred interest in the field of magnetism [2]. Demonstrated to serve as components in memory storage devices, specifically in racetrack memories, these magnetic skyrmions are a significant development. Another notable phenomenon in the field is the Kondo effect [3]. The Kondo effect involves monitoring the resistivity of a metal in relation to temperature. Intriguingly, the metal's resistance reaches a minimum at lower temperatures. Although Kondo initially elucidated this minimum using perturbation theory, it was not until the 1970s that a comprehensive understanding of the Kondo effect was achieved [4].

The objective of this thesis is to gain insight into the key elements that constitute magnetic skyrmions within a small system that accurately encompasses the relevant physics. Skyrmions are topological magnetic structures [5], meaning that their topology stabilizes them. This characteristic makes them especially appealing for applications in spintronics and quantum computing, where precise control over the magnetic properties of materials is crucial [6]. These exotic structures are observed in chiral magnets as individual solitons, meaning that they are self-sustaining and propagate through magnetic material, and can form a lattice of solitons. The Dzyaloshinskii-Moriya interaction DMI plays a key role in stabilizing the chiral symmetry of Skyrmions. Owing to its mathematical structure, it promotes an orthogonal arrangement between spins, whereas standard exchange interaction encourages parallel alignment. The interplay between these two leads to the emergence of skyrmions and their non-collinear magnetic ordering [7]. The study of Skyrmions requires the contributions of renowned scientists in the field such as Werner Heisenberg, Pieter Zee-

man, Igor Dzyaloshinskii, and Toru Moriya, who developed theories of exchange interaction, Zeeman interaction, and Dzyaloshinskii-Moriya interaction, respectively [8].Typically, the investigation of magnetism employs classical models, for instance, the Landau-Lifshitz-Gilbert equation, where only the magnetic moments are simulated. However, it is rare for magnetic moments in a solid to be isolated. More commonly, they coexist with free or itinerant electrons. In this context, a Kondo-lattice model is utilized – which has been demonstrated to give rise to novel physical phenomena.[9].

This project aims to investigate a simple model that includes all the relevant interactions giving rise to a Skyrmion. The system considered is finite and closed. It consists of two interacting spin 1/2 magnetic moments that interact through exchange and DMI, in addition to interacting with a tunable magnetic field. Additionally, an itinerant electron is coupled to the system and described using a Kondo-like interaction. After fully setting up the system quantum mechanically, numerical simulations were performed in order to reveal the time evolution of the spins when varying the parameters. However, a primary objective is to observe the time evolution of the spins when they are described in a mixed quantum-classical picture. This is done by treating one or both of the spins classically using the Ehrenfest approximation, while the electron remains quantum mechanical. The advantage of describing the spins system classically, is the acceleration of computation which becomes important for larger system size. This model was proposed in [10] on a larger lattice, and it was later shown that it could be derived from a two-band Hubbard model [11]. By studying this simple model as a starting point, the aim is to gain insights into the fundamental processes that govern skyrmion systems with larger numbers of interacting particles. The simplicity of the model allows for more manageable computations while still capturing essential features that can potentially be scaled up or extrapolated to more complicated systems. The groundstate of the system will be determined and time-evolved using the Landau-Lifshitz-Gilbert (LLG) equation, predictor-corrector methods, and finally, the Depond-Mertens integration method. This work will provide insight into the accuracy and precision of the different semi-classical models compared to the fully quantum one. In particular, how well the different approaches work as a function of the different interaction strengths within the system.Nonetheless, potential future work may involve establishing a relationship between the entanglement and the precision of the classical approximation.

Chapter 2

Theory and Procedure

2.1 The Quantum Description

In the quantum picture of this work, the system under consideration comprises two fixed spin-1/2 states, an itinerant electron, and a magnetic field. This system is described by the following Hamiltonian:

$$\begin{aligned}\hat{\mathscr{H}} = \quad & J(\hat{\mathbf{S}}_1 \cdot \hat{\mathbf{S}}_2) \\ & +\vec{\mathbf{B}} \cdot (\hat{\mathbf{S}}_1 + \hat{\mathbf{S}}_2) \\ & +\vec{\mathbf{D}}_{12} \cdot (\hat{\mathbf{S}}_1 \times \hat{\mathbf{S}}_2) \\ & +v\left(\hat{c}^{\dagger}_{1\uparrow}\hat{c}_{2\uparrow} + \hat{c}^{\dagger}_{2\uparrow}\hat{c}_{1\uparrow} + \hat{c}^{\dagger}_{1\downarrow}\hat{c}_{2\downarrow} + \hat{c}^{\dagger}_{2\downarrow}\hat{c}_{1\downarrow}\right) \\ & +K\left(\hat{\mathbf{S}}_1 \cdot \hat{\mathbf{s}}_1 + \hat{\mathbf{S}}_2 \cdot \hat{\mathbf{s}}_2\right) .\end{aligned} \tag{2.1}$$

where $\hat{\mathbf{S}}_1$ and $\hat{\mathbf{S}}_2$ represent the two fixed spin-1/2 states while $\hat{\mathbf{s}}_1$ and $\hat{\mathbf{s}}_2$ represent the spin of the itinerant electron at the site of each of the fixed spin-1/2 states. In further detail, the first term in the Hamiltonian represents the Heisenberg exchange between the two spin states, while the second term represents the coupling of the external magnetic field with the spin states, i.e. the Zeeman interaction. The third term represents the Dzyaloshinskii-Moriya interaction, and the last two terms represent the coupling between the fixed spin states and an itinerant electron in accordance to the tight binding model, where this term is similar to the Kondo-like exchange. It is worth noting that, in principle, the external field $\vec{B}$ should also act on the itinerant electron, but, given the educational nature and purpose of the model, such additional interaction is not considered.

In the following subsections, the different terms in the above Hamiltonian will be discussed.

2.1.1 Heisenberg Exchange

In the context of a lattice spin system, the exchange interaction in the Quantum Heisenberg model refers to the interaction between the spins of neighboring particles in the lattice. In a lattice structure, magnetic moments are organized in a regular pattern, and each moment interacts with its neighboring moment to first approximation. The exchange interaction among these moments, a result of the wavefunction's anti-symmetry and Coulomb interaction, plays a crucial role in establishing magnetic order in solids. The constant J in equation (2.1) is the exchange coupling constant, which characterizes the strength of the interaction, and $\hat{\mathbf{S}}_1$ and $\hat{\mathbf{S}}_2$ are the spin operators of two interacting particles 1 and 2.
The exchange interaction between two neighboring spins can have different strengths and directions depending on the nature of the particles and their relative positions in the lattice. For example, in a ferromagnetic material, the coupling constant J between neighboring spins is negative, which means that it favors the alignment of the spins in the same direction. This leads to the formation of a net magnetic moment and the appearance of ferromagnetic ordering. Expanding the first term of the Hamiltonian in equation (2.1) yields

$$\hat{\mathscr{H}}_{\mathrm{HE}} = \quad = \frac{J}{4}\left(2(\hat{\mathbf{S}}_1^{+}\hat{\mathbf{S}}_2^{-}) + 2(\hat{\mathbf{S}}_1^{-}\hat{\mathbf{S}}_2^{+}) + \hat{\mathbf{S}}_1^{z}\hat{\mathbf{S}}_2^{z}\right), \tag{2.2}$$

where the x and y components of the spin operators were rewritten in terms of spin ladder operator.
In order to express $\hat{\mathscr{H}}_{\mathrm{HE}}$ in matrix form, one can use the relation

$$\hat{A} = \sum_{ij} |a_i\rangle A_{ij} \langle a_j| \tag{2.3}$$

and

$$A_{ij} = \langle a_i|\hat{A}\,|a_j\rangle\,. \tag{2.4}$$

where $A_{ij} = \langle a_i|\hat{A}\,|a_j\rangle$ is the matrix element of $\hat{A}$ in the basis $|a_j\rangle$. Here, $\hat{A}$ is an arbitrary operator and $|a_j\rangle$ corresponds to a basis from a set of bases. The ordered bases used for the construction of the 4×4 matrix representation of the different operators for the two spin spaces are $\{|\uparrow\uparrow\rangle, |\uparrow\downarrow\rangle, |\downarrow\uparrow\rangle, |\downarrow\downarrow\rangle\}$. The matrix representation of the Heisenberg exchange

interaction is consequently

$$\hat{\mathscr{H}}_{\mathrm{HE}} = \frac{J\hbar^2}{4}\begin{pmatrix} 1 & 0 & 0 & 0 \\ 0 & -1 & 2 & 0 \\ 0 & 2 & -1 & 0 \\ 0 & 0 & 0 & 1 \end{pmatrix}. \tag{2.5}$$

2.1.2 Zeeman Interaction

The second term of equation (2.1) represents the Zeeman effect, which describes the energy splitting of atomic or molecular energy levels in the presence of an external magnetic field. This effect is significant in the context of magnetically ordered materials, as it can influence the alignment of the magnetic moments of their constituent particles, for example altering the disposition of the magnetic domain. The Zeeman interaction term can be expressed in matrix form, following the same procedure as earlier, as the sum of

$$\hat{\mathscr{H}}_{Bx} = \frac{B_x\hbar}{2}\begin{pmatrix} 0 & 1 & 1 & 0 \\ 1 & 0 & 0 & 1 \\ 1 & 0 & 0 & 1 \\ 0 & 1 & 1 & 0 \end{pmatrix}, \tag{2.6}$$

$$\hat{\mathscr{H}}_{By} = \frac{B_y\hbar}{2i}\begin{pmatrix} 0 & 1 & 1 & 0 \\ -1 & 0 & 0 & 1 \\ -1 & 0 & 0 & 1 \\ 0 & -1 & -1 & 0 \end{pmatrix}, \tag{2.7}$$

and

$$\hat{\mathscr{H}}_{Bz} = B_z\hbar\begin{pmatrix} 1 & 0 & 0 & 0 \\ 0 & 0 & 0 & 0 \\ 0 & 0 & 0 & 0 \\ 0 & 0 & 0 & -1 \end{pmatrix}. \tag{2.8}$$

2.1.3 Dzyaloshinskii-Moriya Interaction

The DMI is also an exchange interaction, but is anti-symmetric in character and arises in magnetic materials with broken inversion symmetry [12]. More clearly, broken inversion

symmetry refers to the lack of symmetry under inversion, which is the transformation that involves reversing the positions of all particles in a system with respect to a central point. Magnetic materials can exhibit broken inversion symmetry due to a variety of factors, such as crystal symmetry, surface or interface effects, or external fields. For example, in thin films or multilayer structures, the interfaces can break the inversion symmetry, leading to the appearance of the DMI and the formation of skyrmions.
The DMI energy favors a particular direction of the magnetization relative to the spin direction, resulting in a non-uniform spin configuration.
In equation (2.1), the vector $\vec{\mathbf{D}}_{12}$ represents the strength of the DMI where $\vec{\mathbf{D}}_{11}$ and $\vec{\mathbf{D}}_{22} = 0$, while $\vec{\mathbf{D}}_{21} = -\vec{\mathbf{D}}_{12}$. The whole DMI term can be expanded as

$$\begin{aligned}\hat{\mathscr{H}}_{\mathrm{DM}} &= \vec{\mathbf{D}}_{12} \cdot \left(\hat{\mathbf{S}}_1 \times \hat{\mathbf{S}}_2\right) \\ &= D_x \left(\hat{\mathbf{S}}_1^y \hat{\mathbf{S}}_2^z - \hat{\mathbf{S}}_1^z \hat{\mathbf{S}}_2^y\right) + D_y \left(\hat{\mathbf{S}}_1^z \hat{\mathbf{S}}_2^x - \hat{\mathbf{S}}_1^x \hat{\mathbf{S}}_2^z\right) + D_z \left(\hat{\mathbf{S}}_1^x \hat{\mathbf{S}}_2^y - \hat{\mathbf{S}}_1^y \hat{\mathbf{S}}_2^x\right) .\end{aligned} \tag{2.9}$$

Substituting in spin ladder operator to the expression gives

$$\begin{aligned}\vec{\mathbf{D}}_{12} \cdot \left(\hat{\mathbf{S}}_1 \times \hat{\mathbf{S}}_2\right) = \quad & \frac{D_x}{2i} \left(\hat{\mathbf{S}}_1^+ \hat{\mathbf{S}}_2^z - \hat{\mathbf{S}}_1^- \hat{\mathbf{S}}_2^z - \hat{\mathbf{S}}_1^z \hat{\mathbf{S}}_2^+ + \hat{\mathbf{S}}_1^z \hat{\mathbf{S}}_2^-\right) \\ & + \frac{D_y}{2} \left(\hat{\mathbf{S}}_1^z \hat{\mathbf{S}}_2^+ + \hat{\mathbf{S}}_1^z \hat{\mathbf{S}}_2^- - \hat{\mathbf{S}}_1^+ \hat{\mathbf{S}}_2^z - \hat{\mathbf{S}}_1^- \hat{\mathbf{S}}_2^z\right) \\ & + \frac{D_z}{4i} \left(-\hat{\mathbf{S}}_1^+ \hat{\mathbf{S}}_2^- + \hat{\mathbf{S}}_1^- \hat{\mathbf{S}}_2^+ - \hat{\mathbf{S}}_1^+ \hat{\mathbf{S}}_2^- + \hat{\mathbf{S}}_1^- \hat{\mathbf{S}}_2^+\right) ,\end{aligned} \tag{2.10}$$

which can be written in matrix form as

$$\hat{\mathscr{H}}_{\mathrm{DM}} = \frac{\hbar^2}{4} \begin{pmatrix} 0 & (iD_x + D_y) & (-iD_x - D_y) & 0 \\ (-iD_x + D_y) & 0 & 2iD_z & (iD_x + D_y) \\ (iD_x - D_y) & -2iD_z & 0 & (-iD_x - D_y) \\ 0 & (-iD_x + D_y) & (iD_x - D_y) & 0 \end{pmatrix} . \tag{2.11}$$

2.1.4 Adding Kondo-like Interactions to the Model

As already briefly mentioned in the introduction, the Kondo effect arises from the interaction between the localized magnetic moments of the impurities and the conduction electrons in the host metal. The Kondo interaction leads to the formation of a many body state known

as Kondo-singlet, where the impurity spin and the surrounding conduction electrons are coupled in a non-perturbative way. This state is responsible for the increase in resistivity at low temperatures, as it effectively scatters the conduction electrons.
A straightforward extension of the Kondo model is its lattice counterpart (Kondo-lattice model). While the Kondo model describes a single magnetic impurity (a localized spin-1/2 particle) interacting with itinerant, non-mutually interacting electrons, the Kondo lattice model considers an array of such magnetic impurities, each interacting with the itinerant electrons. In this model, the electronic structure of the metal is represented by a set of localized orbitals, each capable of holding one electron, akin to a tight binding description. The itinerant electron is then represented as a linear combination of these localized orbitals. The Hamiltonian for this model includes terms that describe the itinerant electron's state and the interaction between the localized spin states and the itinerant electron. Explicitly, in equation (2.1) the 'v' term corresponds to the hopping strength and the 'K' term corresponds to the coupling strength between the electron and the localized spin states.
For the simple case of a spin-dimer plus one electron (i.e. Fig. 2.1), the Kondo Hamiltonian is a 16×16 matrix due to the direct product of the electron's spin space and the itinerant electron's orbital space, where both are 4×4. Therefore, In order to describe the entire system completely, the system's Hamiltonian must be sixteen dimensional. This means that the Hamiltonian in equation (2.1) must have a 16×16 matrix representation. Thus, one need to transform the 4×4 matrix representations of the previously obtained Hamiltonian terms, describing the interaction of the fixed spin states only, to 16×16 matrices. This is done as

$$\hat{\mathscr{H}}^{(16\times16)}_{\text{Total}} = \hat{\mathscr{H}}^{(4\times4)}_{\text{Spin}} \otimes \mathbb{I}^{(4\times4)}_{\text{Electron}} + \mathbb{I}^{(4\times4)}_{\text{Spin}} \otimes \hat{\mathscr{H}}^{(4\times4)}_{\text{Electron}} + \hat{\mathscr{H}}^{(16\times16)}_{\text{S-E Interaction}} . \tag{2.12}$$

2.1.5 Quantum Dynamics

After obtaining the expression for the matrix representation of the total Hamiltonian, one can study the the time evolution of the expectation value of the total spin of the system. The expectation value of an arbitrary operator $\hat{A}$ is given by

$$\langle \hat{A} \rangle = \langle \lambda(t) | \hat{A} | \lambda(t) \rangle . \tag{2.13}$$

where $|\lambda(t)\rangle$ is the state of the system at time t. For a time independent Hamiltonian,

$$i\hbar \frac{\partial |\Psi(t)\rangle}{\partial t} = \hat{\mathscr{H}} |\Psi(t)\rangle \implies |\Psi(t)\rangle = e^{\frac{-i\hat{\mathscr{H}}t}{\hbar}} |\Psi(0)\rangle , \tag{2.14}$$

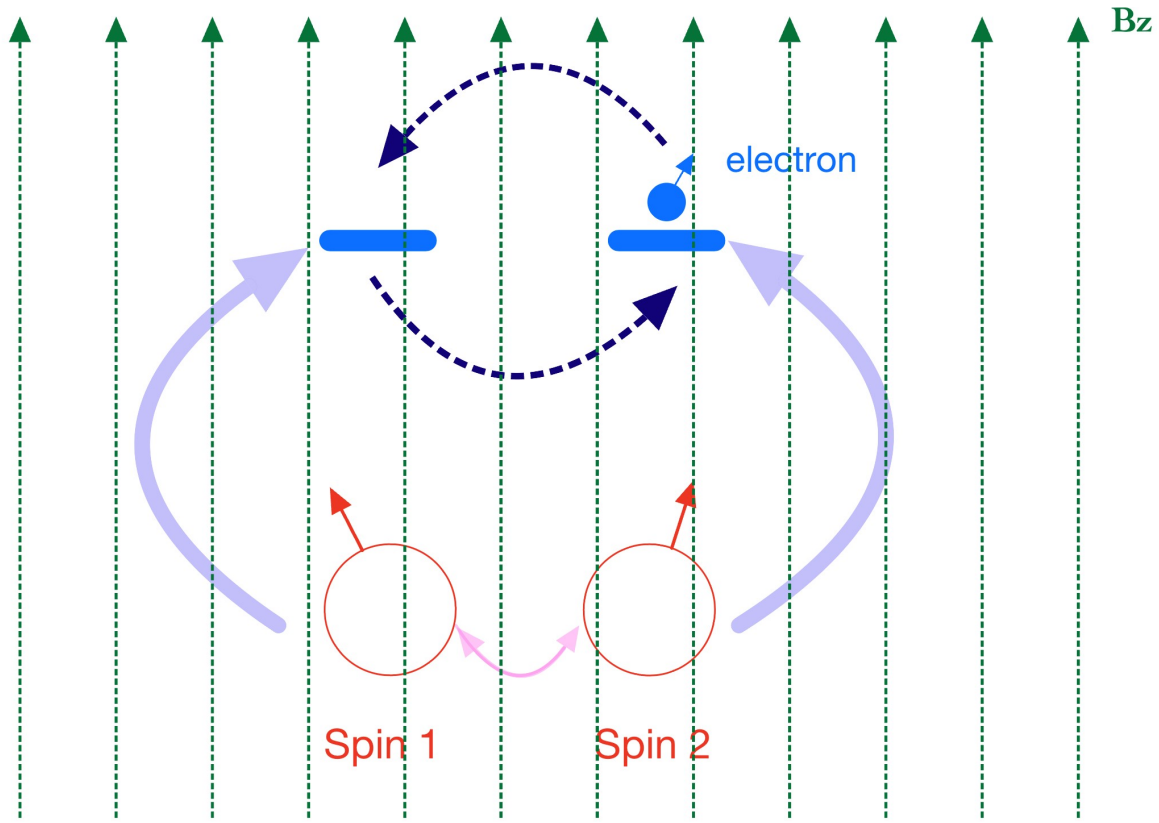

Fig. 2.1: Schematic of the system where two fixed spin states are coupled to each other through exchange and DMI, as well as to a magnetic field and to an itinerant electron. Note that in principle the external field B should also act on the itinerant electron, but, given the educational nature and purpose of the model, such additional interaction is not considered.

where $|\Psi\rangle$ is an arbitrary state. If $|\Psi\rangle$ is an eigenstate of the Hamiltonian, then equation (2.14) can be rewritten as

$$e^{\frac{-i\mathscr{H}t}{\hbar}}|\Psi(0)\rangle = e^{\frac{-iE_\lambda t}{\hbar}}|\lambda(0)\rangle\ , \tag{2.15}$$

where E_λ is the eigenenergy corresponding to the eigenstate $|\lambda\rangle$. However, for the case of a time dependent Hamiltonian, $\hat{\mathscr{H}}(t)$, a state $|\Psi(t)\rangle$ evolves from time t to time $t+\Delta$ as

$$|\Psi(t+\Delta)\rangle = \sum_\lambda \exp\left(\frac{-iE_\lambda(t+\delta)\Delta}{\hbar}\right)|\lambda\,(t+\delta)\rangle\,\langle\lambda\,(t+\delta)|\Psi(t)\rangle\ , \tag{2.16}$$

where $\delta = \frac{\Delta}{2}$. In equation (2.16), the implicit assumption is that Δ is sufficiently small and the mid point method is utilized to numerically converge faster to the expectation values of different operators.

2.1.6 Application of Hellman-Feynman Theorem

The Hellman-Feynman theorem provides a useful tool for validating the numerical robustness of the computed expressions for the various Hamiltonian terms. This theorem, with the given Hamiltonian and its corresponding eigenfunctions, can be expressed as:

$$\langle \lambda | \frac{\partial \hat{\mathscr{H}}}{\partial A} | \lambda \rangle = \lim_{\varepsilon \to 0} \frac{E(A+\varepsilon) - E(A)}{\varepsilon} \,. \tag{2.17}$$

In the above equation, A represents one of the adjustable parameters of the Hamiltonian, and E signifies an eigenvalue of the Hamiltonian. The validation process involves a comparison of the left-hand side, derived analytically, with the right-hand side, computed numerically. A match between these two sides affirms the correctness of the expressions.

2.2 The Classical Description

In this thesis, the primary goal of studying the classical representation of the system is to compare its outcomes to those of the quantum representation. More in detail, the full quantum solution will be compared to a classical treatment described by the Ehrenfest approximation.

2.2.1 Ehrenfest Theorem

The Ehrenfest theorem, which is named after Paul Ehrenfest, connects the rate of change over time of the expectation values of position and momentum operators, denoted by $\hat{x}$ and $\hat{p}$, to the expectation value of force. However, this theorem is a special case of a more general equation [13] defined by

$$\left\langle \frac{\partial \hat{A}}{\partial t} \right\rangle = \frac{1}{i\hbar} \left\langle [\hat{A}, \hat{\mathscr{H}}] \right\rangle + \frac{\partial}{\partial t} \langle \hat{A} \rangle \,, \tag{2.18}$$

where $\hat{A}$ is an arbitrary operator. For a time independent operator the last term in equation (2.18) is trivially equal to zero.
The evaluation of equation (2.18) for the different spin components of each spin state and

Hamiltonian from (2.1) yields

$$\begin{aligned}
\frac{1}{i\hbar}[\hat{\mathbf{S}}_1^x, \hat{\mathscr{H}}] &= -J(\hat{\mathbf{S}}_1 \times \hat{\mathbf{S}}_2)_x - (\hat{\mathbf{S}}_1 \times \vec{B})_x - (\hat{\mathbf{S}}_1 \times (\vec{D} \times \hat{\mathbf{S}}_2))_x - K(\hat{\mathbf{S}}_1 \times \hat{\mathbf{s}}_1)_x \\
\frac{1}{i\hbar}[\hat{\mathbf{S}}_1^y, \hat{\mathscr{H}}] &= +J(\hat{\mathbf{S}}_1 \times \hat{\mathbf{S}}_2)_y + (\hat{\mathbf{S}}_1 \times \vec{B})_y + (\hat{\mathbf{S}}_1 \times (\vec{D} \times \hat{\mathbf{S}}_2))_y + K(\hat{\mathbf{S}}_1 \times \hat{\mathbf{s}}_1)_y \\
\frac{1}{i\hbar}[\hat{\mathbf{S}}_1^z, \hat{\mathscr{H}}] &= -J(\hat{\mathbf{S}}_1 \times \hat{\mathbf{S}}_2)_z - (\hat{\mathbf{S}}_1 \times \vec{B})_z - (\hat{\mathbf{S}}_1 \times (\vec{D} \times \hat{\mathbf{S}}_2))_z - K(\hat{\mathbf{S}}_1 \times \hat{\mathbf{s}}_1)_z
\end{aligned} \tag{2.19}$$

The Ehrenfest approximation of the x, y and z terms for the time derivative of $\hat{\mathbf{S}}_1$ can be collected together as

$$\frac{\partial}{\partial t}\vec{\mathbf{S}}_1(t) = \frac{1}{i\hbar}[\vec{\mathbf{S}}_1, \hat{\mathscr{H}}] = -J(\vec{\mathbf{S}}_1 \times \vec{\mathbf{S}}_2) - (\vec{\mathbf{S}}_1 \times \vec{B}) - (\vec{\mathbf{S}}_1 \times (\vec{D} \times \vec{\mathbf{S}}_2)) - K(\vec{\mathbf{S}}_1 \times \langle\vec{\mathbf{s}_1}\rangle)\,, \tag{2.20}$$

where the spin operators of the fixed spin-1/2 states have been rewritten into vector form. One should also note that in order to incorporate the expression for the electron, which is quantum mechanical, one needs to introduce it in vector form. This is done by taking its expectation value as $\langle\vec{\mathbf{s}_1}\rangle$, as seen in the above equation. This is primarily due to the fact that The electronic spin, which is quantum mechanical, is represented in vector form by deducing its expectation value in the x, y and z directions. Moreover, for consistency, a constraint is required such that the length of the spins must remain constant. Physically, the modulus of the fermionic spins is fixed at one-half. However, for the sake of numerical convenience, they are treated as if they are bounded by positive and negative one, while keeping in mind their inherent directionality and rotation properties. Repeating the same procedure with $\vec{\mathbf{S}}_2$ gives a final set of coupled equations which describe the dynamics of the spins as

$$\boxed{\begin{aligned}
\frac{\partial}{\partial t}\vec{\mathbf{S}}_1(t) &= -\vec{\mathbf{S}}_1 \times \left(J \cdot \vec{\mathbf{S}}_2 + \vec{B} + (\vec{D} \times \vec{\mathbf{S}}_2) - K \cdot \langle\vec{\mathbf{s}}_1\rangle\right) \\
\frac{\partial}{\partial t}\vec{\mathbf{S}}_2(t) &= -\vec{\mathbf{S}}_2 \times \left(J \cdot \vec{\mathbf{S}}_1 + \vec{B} - (\vec{D} \times \vec{\mathbf{S}}_1) - K \cdot \langle\vec{\mathbf{s}}_2\rangle\right) \\
\left|\vec{\mathbf{S}}_i(t)\right| &= 1, \quad \forall i, \forall t\,.
\end{aligned}} \tag{2.21}$$

2.2.2 The Landau–Lifshitz–Gilbert Equation

There is an equivalence worth mentioning between the expression obtained in 2.21 and the Landau–Lifshitz–Gilbert (LLG) equation. The LLG equation is a differential equation used to describe the precessional motion of magnetization in solids and to model the time

evolution of magnetic elements due to a magnetic field [14]. The LLG equation is given as

$$\frac{d\vec{M}}{dt} = -\gamma\left(\vec{M}\times\vec{H}_{\text{eff}} - \alpha\vec{M}\times\frac{d\vec{M}}{dt}\right), \tag{2.22}$$

where $\vec{M}$ is the magnetization γ is the gyro-magnetic ration α is the Gilbert damping parameter and $\vec{H}_{\text{eff}}$ is the effective field/force. The equivalence can be more clearly seen if one treats the term $\left(J\cdot\vec{\mathbf{S}}_i + \vec{B} + (\vec{D}\times\vec{\mathbf{S}}_i) - K\cdot\langle\vec{\mathbf{s}}_j\rangle\right)$ as the effective field $\vec{H}_{\text{eff}}$; as well as the spins with the magnetization. The damping term in the LLG equation is introduced to account for the dissipation of energy due to the interaction of the magnetic moment with its environment, such as thermal fluctuations or the interaction with the surrounding lattice or electrons. The damping term ensures that the magnetic moment eventually relaxes to its equilibrium state and prevents the magnetic moment from precessing indefinitely.
However it may be useful to note that, while formally resembling the LLG equation, the spin equation in (2.21) directly emerges from the classical limit of the Heisenberg equation of motion for the spin operators and in our treatment is supplemented by the electron dynamics.

2.2.3 Numerical Integration Theory

Precession

In order to numerically calculate the value of a variable at a given time step δt, one often resorts to solving first order differential equations of the form

$$\mathbf{S}_i(t+\delta t) = \mathbf{S}_i(t) + \dot{\mathbf{S}}_i(t)\delta t\,, \tag{2.23}$$

using Euler integration schemes. However, such integrations prove to be unsuitable for the cases where a constraint on the length of the variable exists. The proof of the inconsistency of Euler method integration can be seen in the following expansion where

$$\begin{aligned}|\mathbf{S}_i(t+\delta t)|^2 &= \left|\mathbf{S}_i(t) + \dot{\mathbf{S}}_i(t)\delta t\right|^2 \\ &= |\mathbf{S}_i(t)|^2 + 2\mathbf{S}_i(t)\cdot\dot{\mathbf{S}}_i(t)\delta t + \left|\dot{\mathbf{S}}_i(t)\delta t\right|^2 \\ &= |\mathbf{S}_i(t)|^2 + \left|\dot{\mathbf{S}}_i(t)\delta t\right|^2 .\end{aligned} \tag{2.24}$$

This shows that the length of the spin increases in both systematic and nonphysical ways. Hence, a better approach is required to complete the integration of the spins. A suitable integration method was proposed by Ph Depondt and F G Mertens in [15]. Their technique is

based on precession which can be explicitly carried out using the Rodrigues equation which enables the computation of the rotation of a vector about a field. Formally, the rotation is carried out by having

$$\vec{\mathbf{S}}_i(t+\delta t) = \mathbf{R}_i(t)\vec{\mathbf{S}}_i(t)\,, \tag{2.25}$$

where the rotation matrix is

$$\mathbf{R}_i(t) = \begin{pmatrix} h_x^2 u + \cos\omega & h_x h_y u - h_z \sin\omega & h_x h_z u + h_y \sin\omega \\ h_x h_y u + h_z \sin\omega & h_y^2 u + \cos\omega & h_y h_z u - h_x \sin\omega \\ h_x h_z u - h_y \sin\omega & h_y h_z u + h_x \sin\omega & h_z^2 u + \cos\omega \end{pmatrix}. \tag{2.26}$$

In the rotation matrix above, $u = 1 - \cos\omega$ whereas h_x, h_y, h_z are the coordinates of the unit vector $\mathbf{h} = \mathbf{H}_i / |\mathbf{H}_i|$. Here $\mathbf{H}_i$ is the corresponding effective field of $\vec{\mathbf{S}}_i(t)$. Notably, the vector $\mathbf{h}$ is parallel to the local field and the precession angle $\omega = |\mathbf{H}_i|\,\delta t$. Hence the spin length remains constant up to numerical accuracy, as prescribed by equation (2.21).

Predictor-Corrector Method

The predictor-corrector method is a a type of numerical multistep method within the category of hybrid methods [16]. General predictor-corrector methods are a type of numerical integration methods that use a combination of predictor and corrector stages to approximate the solution of a differential equation. In general, these methods are multistage, meaning that they involve multiple steps to predict and correct the solution at each time step.
In the predictor stage, a lower order approximation is used to estimate the solution at the next time step. This approximation may not be exceptionally accurate, but it is relatively useful when solving self-consistent problems. The corrector stage, on the other hand, uses a higher order approximation to refine the estimate obtained from the predictor stage. The resulting approximation is generally more accurate, but may require more computation time and memory than the predictor stage.
The use of both predictor and corrector stages allows general predictor-corrector methods to balance efficiency and accuracy in a flexible way, making them useful for a wide range of problems. These methods are particularly effective for solving problems that have oscillatory or periodic behavior, where more traditional numerical methods may struggle.

Nelder-Mead Minimization

In addition to the LLG equation, which incorporates Gilbert damping to enable the relaxation of a system towards its ground state, minimization techniques such as the Nelder-Mead

algorithm can be employed. The Nelder-Mead algorithm is a direct search optimization algorithm that determines the minimum of a function without utilizing gradients[17]. The algorithm operates iteratively, starting with an initial simplex, and then adjusting the simplex until convergence to a local minimum is achieved. In this work, the Nelder-Mead algorithm can be applied to identify the spin coordinates corresponding to the system's lowest energy, given specific parameters such as the spins' coupling strength, denoted as J in equation (2.1), and others.
The Hamiltonian function, which provides the energy of the system, takes into consideration various interactions between individual spins in a dimer and the external magnetic field acting on the system. By minimizing the Hamiltonian function with respect to the spin configuration, the equilibrium configuration of the system and its corresponding energy can be determined. This energy function can then be minimized using the Nelder-Mead method to find the lowest energy configuration of the system. The error of this function depends on the absolute error in the input variables and the function value. However, it is worth noting that the Nelder-Mead method is not guaranteed to converge to the global minimum, particularly for high-dimensional functions. While it can often find a satisfactory solution, it does not provide strong guarantees regarding global optimality or the accuracy of the solution.

2.3 The Numerical Procedure

The results of the computationally implemented model were validated by introducing the different Hamiltonian terms step by step, and comparing the obtained results against the analytical expectations. Thereafter, the time evolution of the full system was studied, with the details described in the following subsections.

2.3.1 Quantum

In this part, where the whole system is treated quantum mechanically (QQ) , the total Hamiltonian of the system was constructed and the time evolution of the systems were computationally implemented using Python. The groundstate was obtained through the diagonalization of the Hamiltonian, which was then numerically propagated in time using the algorithm described in equation (2.16). At each time step, the expectation value of the spins and energy were taken using the relation in equation (2.13).

2.3.2 Semi-Classical

The approach here was to combine the different techniques and theories prescribed in section 2.2.3 to create the desired algorithm. In the first case, the algorithm was created for a system with two classical spins and a quantum electron (CC) . In the other case, one of the spins was quantum while the other was classical (QC). The procedure for having (CC) is as follows:

- Create initial spin states $\vec{\mathbf{S}}_1^{(0)}$ and $\vec{\mathbf{S}}_2^{(0)}$ by minimizing the Hamiltonian function of the system using the Nelser-Mead method.
- Define a function that takes the parameters and the initial spin states as inputs.
- Create containers in the function to store the value of the spins and energy at each time step.
- Initialize the electron's groundstate and its average spins, $\langle \vec{\mathbf{s}}_1 \rangle$ and $\langle \vec{\mathbf{s}}_2 \rangle$, within the function. At this point, all the terms of equation (2.21) are now computed.
- Start an iteration where in each time step:
    1. Express the effective fields for each spin using the right hand side of equation (2.21) (**H** in equation (2.26)).
    2. **Predict** the electronic wavefunction, by time propagating it as in equation (2.13) using the initial spins, and its average spin at each site.
    3. **Predict** the spins $\vec{\mathbf{S}}_1$ and $\vec{\mathbf{S}}_2$ by using the rotation matrix from equation (2.26) and the effective field.
    4. **Predict** the effective fields, using the predicted spins as well as the right hand side of equation (2.21) (**H** in equation (2.26)).
    5. **Correct** the electronic wavefunction and its average spin using the average of the initial spins and the predicted spins.
    6. **Correct** the effective field using the average of the initial field and the predicted field.
    7. **Correct** the spins $\vec{\mathbf{S}}_1$ and $\vec{\mathbf{S}}_2$ using the average of the initial spins and the predicted field.
    8. Calculate the energy and store its value, alongside the value of the spins, in the containers.
    9. Repeat.

The procedure for the single quantum single classical (QC) on the other hand is identical to the above procedure with the exception that $\vec{\mathbf{S}}_2$ is treated quantum mechanically. That is, initial and time-evolved, both in the predicted an corrected stage, spins are obtained using diagonalization and quantum dynamics in a similar fashion to that of the itinerant electron.

2.3.3 System Parameters and External Fields

The procedures described above were utilized to evaluate the ground state under a variety of parameter conditions. Although a full parameter scan was not performed, for each quantity a large and a small value were used to have a coarse grid of values. The parameters varied were J, B_z, D_z, and K, which were set to -0.2 (representing small values) or -1 (representing large values). Throughout the study, v was consistently maintained at a constant value of -1, while B_x, B_y, D_x, and D_y were all set to 0.

In addition, three distinct perturbations were used for the magnetic field. In detail, a slow perturbation was applied at $t = 5$, with $B_x = B \cdot f(t)$ and $B_z = B$. The value of B determines the strength of the perturbation (-0.2 or -1), while the shape of $f(t)$ determine how the perturbation was applied in time. Three scenarios were considered. The cases of slow and fast ramping correspond to

$$f(t) = \begin{cases} 0, & \text{for} \quad t \leq 5 \\ -\left[\sin\frac{(t-5)\pi}{\tau}\right]^P, & \text{for} \quad 5 \leq t \leq 25 \\ -1, & \text{for} \quad t > 25 \end{cases}, \tag{2.27}$$

where $P = 1$ and $\tau = 40$ for the slow scenario, and $P = 10$ and $\tau = 10$, for the rapid scenario. A third case of sudden ramping was described by $f(t) = -\Theta(t-5)$, where Θ is the step function.

This procedure was executed for two cases, namely $B = 0.2$ (small field) and $B = 1$ (large field). Also, a factor of $\mu_B = -1$, is introduced to the magnetic field term to favor the alignment of the spins to the direction of the magnetic field. Finally, the energy, spins, and electron density of the system were stored during the time evolution.

Chapter 3

Results and Discussion

3.1 Code Testing

Test 1. Considering a simple case involving the Heisenberg exchange and Zeeman interaction with $J = -1$ and $\vec{\mathbf{B}} = (1,0,0)$, a ferromagnetic coupling is expected between the two spins, resulting in their alignment with the magnetic field. The numerical results, as illustrated in Figure 3.1, confirm this behavior.

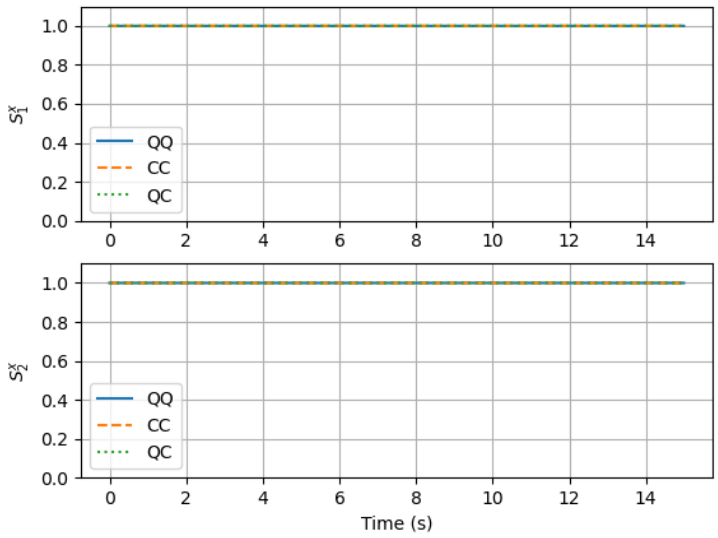

Fig. 3.1: Spin alignment with Heisenberg exchange and Zeeman interaction. The QQ corresponds to the fully quantum approach. QC corresponds to having one spin state classical and the other quantum while CC corresponds to having both spins states classical.

Test 2. Upon introducing electrons to the system with $K = -1$, the electron spins should align

with the spins at each site. Consequently, the electrons should also point in the x-direction, as demonstrated in Figure 3.2.

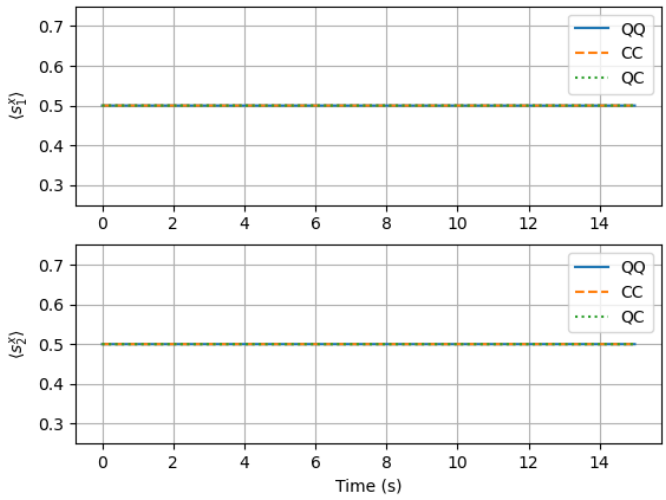

Fig. 3.2: Electron spin alignment in the presence of Heisenberg exchange, Zeeman interaction, and electrons.

Test 3. Incorporating the DMI in the z-direction with $J = -1$ and $\vec{\mathbf{B}} = (1,0,0)$ introduces an asymmetry between $\vec{\mathbf{S}}_1$ and $\vec{\mathbf{S}}_2$. This effect is prominently displayed in Figure 3.3. One can

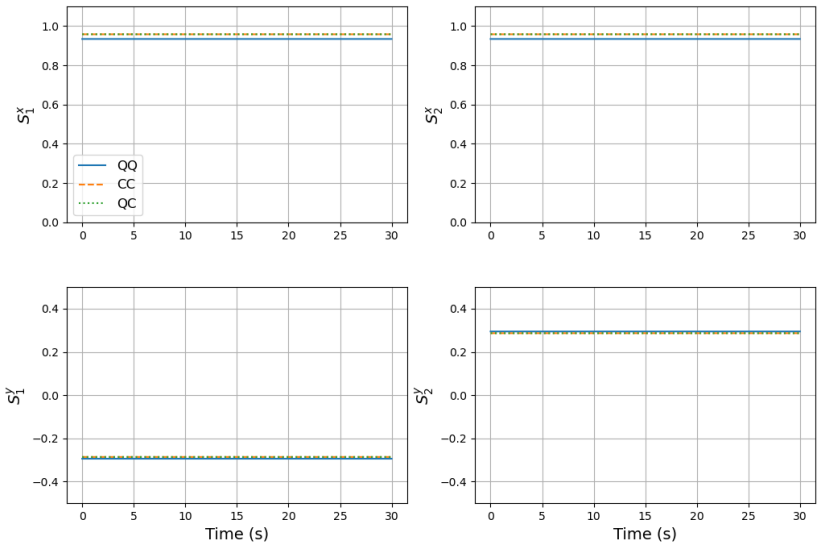

Fig. 3.3: Asymmetry induced by DMI in the y-direction.

also already see a clear discrepancy in the agreement of the groundstate between the fully quantum approach and the semi-classical approaches.

3.2 Time Evolution

In this section, parameters of small value are denoted by lower case letters, while those of large value are denoted by upper case letters. More explicitly, $(J, j) \equiv (-1, -0.2)$, $(D, d) \equiv (-1, -0.2)$, and $(K, k) \equiv (-1, -0.2)$.
It should be noted that b (B) represents simultaneously small (large) B_z and small (large) time dependent perturbations due to B_x. Additionally, as previously mentioned, the DMI term is only acting the z-direction such that D_z is either equal to D or d.
The selected results below are quite representative of all the actual simulations performed and illustrate the the degree of agreement between the double classical (CC) and single quantum single classical (QC) representations compared to the exact solution from the fully quantum (QQ) representation, for different combinations of parameters. In particular, the best and worst agreements for the different perturbations and magnetic field strengths have been picked out and showcased here.

3.2.1 Slow Perturbation in B_x Field

Figure 3.4 shows that when the magnetic field is small, the best agreement is obtained when all the different parameters are small.

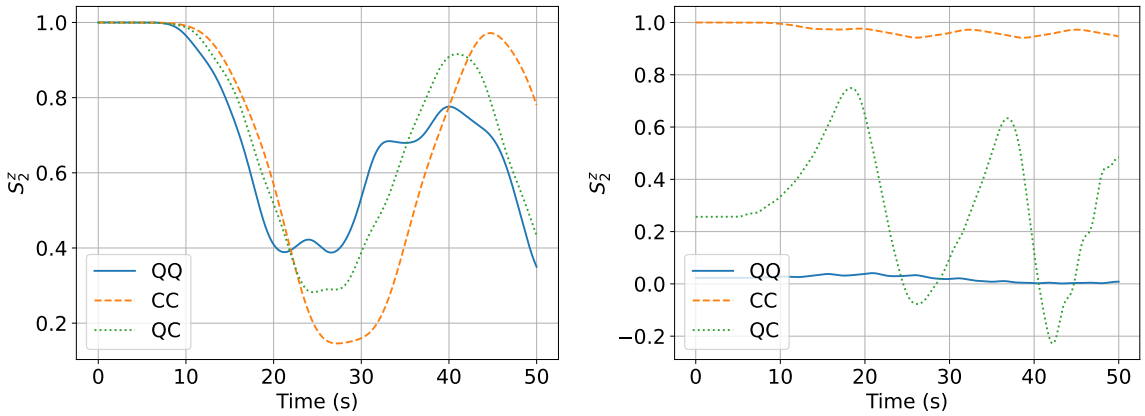

(a) b, d, j, and k - Best agreement

(b) b, D, j, and k - Worst agreement

Fig. 3.4: Comparison of data in small magnetic field and slow perturbation.

However, when the d term alone is switched to the large value D, the agreement deteriorates. It is also noteworthy that the results with poor agreement had the spin starting from different initial values. This indicates that the different models did not produce the same ground state. On the other hand, figure 3.5 shows that when the magnetic field is large, a good agreement is still observed when all parameters are small. Looking more closely, one notices that the (QC) and the (CC) curves follow quite closely the full quantum solution. However, overtones are clearly noticed, in the form of bound oscillations, phase difference, and lying around the quantum solution. Still, the overall agreement is good and this is likely due to the fact that the external magnetic field here is the dominant factor in the determining the system's dynamics.

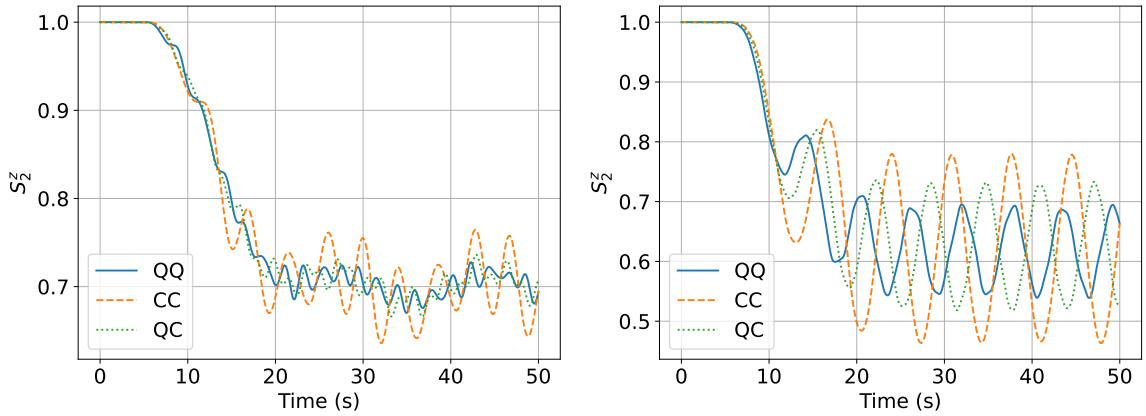

(a) B, d, j, and k - Best agreement

(b) B, D, J, and K - Worst agreement

Fig. 3.5: Comparison of data agreement in large magnetic field and slow perturbation.

When the other system parameters also become large, the agreement becomes deteriorated. One can moreover see that the initial conditions do not match, hence the poor agreement in the time evolution as well.

3.2.2 Rapid Perturbation in B_x Field

As shown in figure 3.6, when the magnetic field is small, the best agreement is achieved when all parameters are small compared to when only the DMI term d is set to a large value. Yet again, an amplitude and phase difference for the best agreement case is witnessed. Also, different initial conditions can once more be seen in the result that gave the worst agreement.

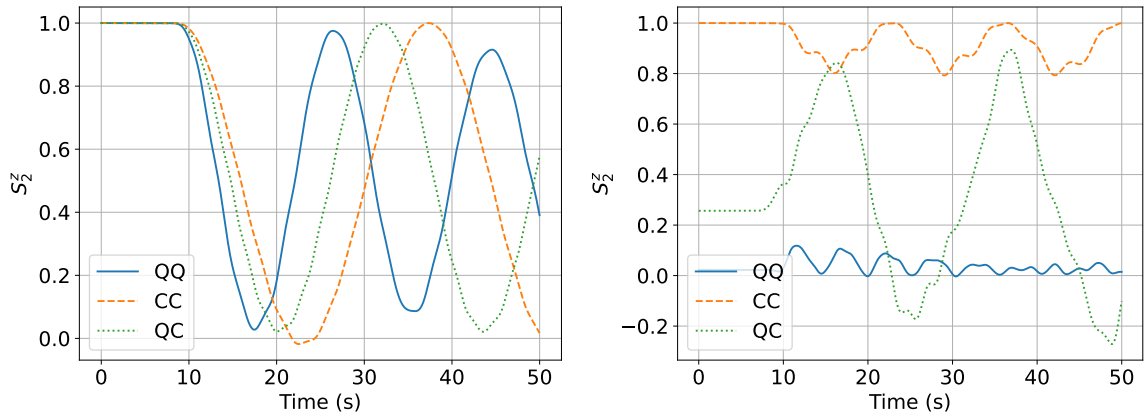

(a) b d, J, and K - Best agreement

(b) b, D, j, and k - Worst agreement

Fig. 3.6: Comparison of data agreement in small magnetic field and rapid perturbation.

For the case of large magnetic field, as in figure 3.7, the best agreement is again observed when all parameters are small, except for K. However, if the DMI is increased and the other parameters are kept small, the agreement worsens.

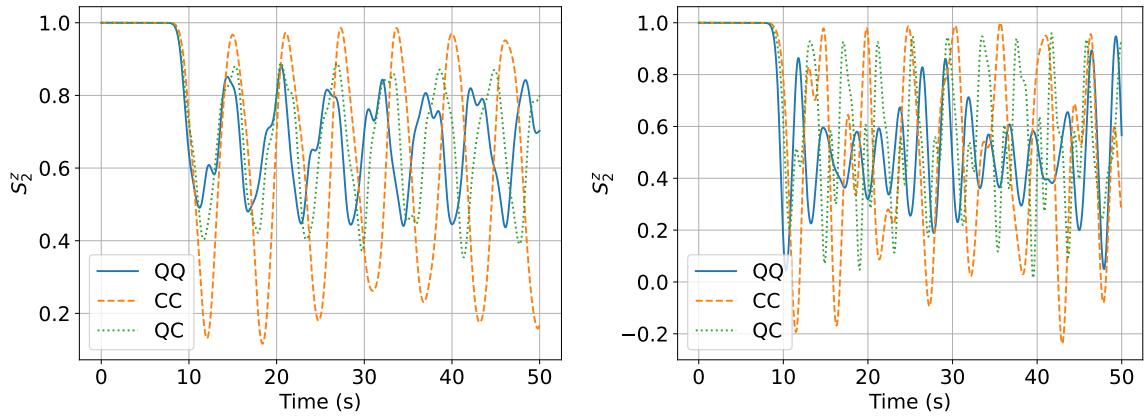

(a) B, d, j, and K - Best agreement

(b) B, D, j, and k - Worst agreement

Fig. 3.7: Comparison of data agreement in large magnetic field and rapid perturbation.

Overall, there is an evident deterioration of the agreement between the different approaches in the rapid perturbation case compared to the results obtained with slow perturbation. Although the common denominator of the results for the two different perturbations is that for the case of having a small magnetic field, the worst agreement are given in the form of different initial conditions. In addition to that, larger magnetic field seem to improve the overall agreement compared to when having a small magnetic field.

3.2.3 Sudden Perturbation in B_x Field

The results from figure 3.8 indicate that for the case of a small magnetic field, the best agreement occurs when all parameters are large, except for d, compared to when the DMI term D is large and the rest are small. Once again, one can see the same features here as in the previous perturbation cases where the best agreement still contain phase and amplitude difference and the worst agreement result is due to different initial conditions.

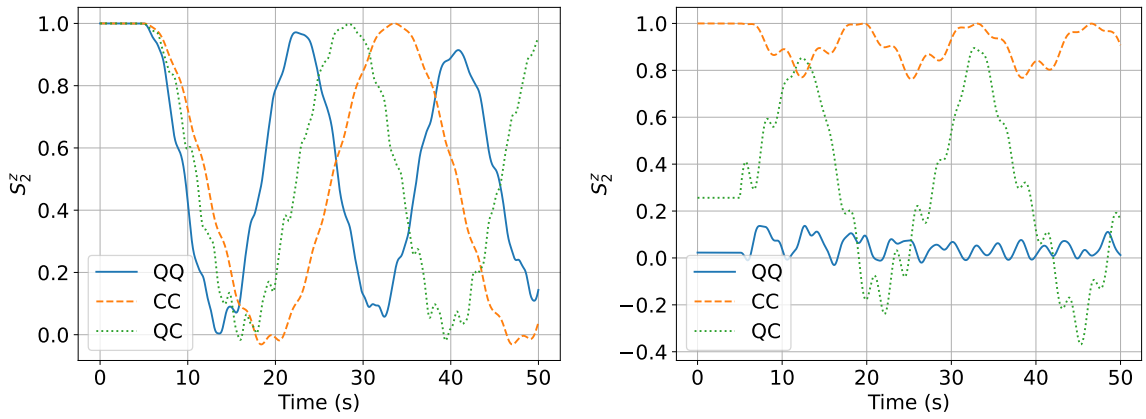

(a) b, d, J, and K - Best agreement

(b) b, D, j, and k - Worst agreement

Fig. 3.8: Comparison of data agreement in small magnetic field and sudden perturbation.

For the case of a large magnetic field better agreement is observed when all the parameters are large, according to the results in figure 3.8. Conversely, when the DMI is set to large and the other terms are small, the agreement becomes poor as shown in figure 3.9.

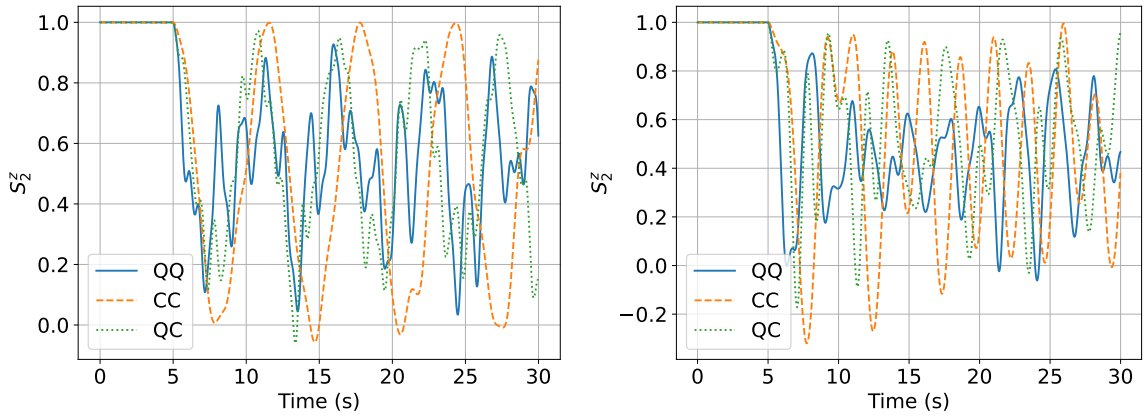

(a) B, D, J, and K - Best agreement

(b) B, D, j, and k - Worst agreement

Fig. 3.9: Comparison of data agreement in large magnetic field and sudden perturbation.

, the overall agreement here seem to be worse than the one with slow perturbation. Although, it is not so clear which perturbation one , rapid or sudden, gives rise to the worst overall agreement. However, it is comprehensible that slow perturbation gives the best overall agreement between three different perturbations used.

3.2.4 Discussion

The results presented above are a representative subset of a total of $3 \cdot 2^4$ results, wherein different combinations of small and large valued parameters are utilized, along with different approaches to apply perturbation. As a general observation, the results clearly indicate that when the DMI term is the dominant interaction, the agreement among the different schemes notably diminishes. When the DMI term is less influential than the others, the results match better. A second general trend is that the agreement is best when the external perturbation is slow. Besides these two general trends, and within the set of simulations performed, it was not immediate to find further general features in the results. Rather, the system showed a highly sensitive and intricate dependence on the value of the different interaction strengths. But mostly, the numerical evidence seemed to indicate that having larger J, smaller K, and larger B (magnetic field) generally improves the agreement.

Another aspect which could have had a significant influence on the quality of the agreement between exact on approximate solutions is related to the ability of finding a correct initial state in the semi-classical approximation. Figures 3.6 and 3.4 reveal the limitations of starting from the Nelder Mead minimized groundstate. Since, already, at $t = 0$ the agreement is poor, which is likely the cause to the disagreement between the fully quantum solution and the two semi-classical ones.

It is also clear that quantum classical solutions generally exhibit better agreement with the exact solution than do classical classical ones, an unsurprising observation given that the exact solution is fully quantum, and quantum classical is a step closer to this compared to the classical classical one.

A likely explanation is that the coherent response and the quantum coherence of the system following the rapid or sudden perturbation, which are fully accounted in the quantum treatment, are not accurately captured by semi-classical treatments. Moreover, such swift perturbations could induce entanglement between the different components of the system, and this is something that mixed quantum-classical methods typically do not account for. Consequently, under rapid or sudden perturbations, the mixed quantum-classical solutions might not align as accurately with the full quantum solutions due to the intricate quantum

effects involved.

In summary, despite some general clear trends were observed (in particular, the DMI reduces the agreement between different treatments), it was not possible to associate easily discernible trends due to the specific impact of all the different interaction terms. It is likely that, to determine in full the conditions under which the quantum-classical or the classical-classical methods perform best, an extensive search in the parameter space would be required, something to be performed in future investigations.

Chapter 4

Conclusion & Outlook

In this dissertation, a theoretical examination of the magnetic behavior of a basic model system featuring various and competing magnetic interactions has been conducted. The model includes two localized magnetic moments (also referred to as spins due to their link to moments through the gyromagnetic ratio) and a single itinerant electron hopping between two orbitals located at the spins' positions.

These stationary spins interact via i) the Heisenberg exchange, which can cause either ferro- or antiferro-magnetic ordering between the spins, depending on its sign, and ii) the Dzyaloshinskii-Moriya interaction (DMI), which results in orientational canting between the spins (DMI arises in non-center-symmetric systems and when spin-orbit interaction is present).

This research had the main objective to characterize the system with various levels of accuracy and compare them. The three different descriptions considered were: a) a full quantum, exact solution, achieved with the configuration interaction method; b) a quantum-classical hybrid solution, where the electron and one of the localized spins are handled quantum-mechanically, while the other spin is handled classically; c) a similar quantum-classical scheme, but where both localized spins are described classically.

Comparing the exact solution and the two quantum-classical descriptions (the latter were obtained within the Ehrenfest approximation), the results indicated that better consistency is achieved at smaller exchange couplings, smaller external magnetic fields, and slow rather than fast perturbations. As expected, the results from the system with a classical spin were closer to the exact solution than those with two classical spins. This pattern applies to spins, electronic densities, and system energies. However, there were a few cases where the trend was reversed (for the system's energy only; we do not currently have an explanation for this behavior).

Why are the findings of this study and possible future research of this nature potentially important? The scientific and technology communities are increasingly becoming aware that magnetic systems hold considerable promise for new, sustainable electronic devices that consume less energy and circumvent Moore's law limitations. This is the ultimate goal of spintronics, a research and technology field focused on spin-based electronics. The magnetic interactions discussed in this thesis form the foundation of many magnetic phenomena and behaviors relevant to spintronics. In our study, we considered a very basic system with these interactions. However, larger systems of the same kind can create highly exotic spin structures, such as topologically protected spin-vortex-like formations called skyrmions, which are highly resilient to perturbations and defects. Skyrmions could be crucial for the development of new data storage processes and have also been explored for quantum information purposes. While significant strides have been made in creating and characterizing skyrmions (and other similarly important magnetic structures) experimentally, a comprehensive theoretical description of general scope still remains a challenge, particularly given that these structures might encompass several thousands of spins, thus making a full quantum description currently impractical. This highlights the necessity for quantum-classical treatments and a thorough examination of the scope and validity of these approximate methods, as carried out in this thesis.
Because of time constraints and the longer-than-expected time to establish the computer code for producing results, we were unable to provide a thorough characterization of our system's parameter space. Similarly, we couldn't pursue some planned conceptual extensions of the work. Moving forward, it would be worthwhile to explore the following directions:

1. Including more than one electron and their interactions.

2. Incorporating more than two localized spins to see how/if the increased "contamination" from classical spins impacts the spin dynamics.

3. Implementing the computation of concurrence (entanglement), a significant indicator of quantum correlations, to observe and quantify the impact of classical contamination on entanglement.

4. Considering the role of dissipation by introducing an explicit oscillator bath to keep the dynamics Hermitian and test the potential limitations of the resulting LLG equation.

5. Exploring the use of an external bath to recover some quantum characteristics in a classical spin assembly.

6. Performing calculations with larger spins (i.e., 1, 3/2, 2, 5/2, etc.) to see how the classical and quantum results converge.

7. Last, but not least, to use fully quantum solutions in small model system, to characterize in rigorously the interplay of different magnetic interaction and how this induces different dynamical magnetic regimes.

These research directions are well within the realm of the methodology presented in this thesis, through obvious and relatively straightforward (though extensive) generalizations. All these, however, are to be tackled in future research.

References

[1] I. S. Jacobs. Role of magnetism in technology. *Journal of Applied Physics*, 40(3):917 – 928, 1969.

[2] S. Mühlbauer, B. Binz, F. Jonietz, C. Pfleiderer, A. Rosch, A. Neubauer, R. Georgii, and P. Böni. Skyrmion lattice in a chiral magnet. *Science*, 323(5916):915 – 919, 200.

[3] Jun Kondo. Resistance Minimum in Dilute Magnetic Alloys. *Progress of Theoretical Physics*, 32(1):37–49, 07 1964.

[4] Kenneth G. Wilson. The renormalization group: Critical phenomena and the kondo problem. *Rev. Mod. Phys.*, 47:773–840, Oct 1975.

[5] Dan Liu, Tongyun Zhao, Ming Zhang, Lichen Wang, Jianfeng Xi, Baogen Shen, Baohe Li, Fengxia Hu, and Jirong Sun. Exploration of nontrivial topological domain structures in the equilibrium state of magnetic nanodisks. *Journal of Materials Science*, 56(7):4677 – 4685, 2021.

[6] *Magnetic Skyrmions. [Elektronisk resurs].* InTech, 2021.

[7] S Mühlbauer, B Binz, F Jonietz, C Pfleiderer, A Rosch, A Neubauer, R Georgii, and P Böni. Skyrmion lattice in a chiral magnet. *Science (New York, N.Y.)*, 323(5916):915 – 919, 2009.

[8] Junichi Iwasaki, Masahito Mochizuki, and Naoto Nagaosa. Current-induced skyrmion dynamics in constricted geometries. 2013.

[9] Rintaro Eto, Rico Pohle, and Masahito Mochizuki. Low-energy excitations of skyrmion crystals in a centrosymmetric kondo-lattice magnet: Decoupled spin-charge excitations and nonreciprocity. 2022.

[10] Emil Viñas Boström and Claudio Verdozzi. Steering magnetic skyrmions with nonequilibrium green's functions. 2018.

[11] Emil Viñas Boström, Angel Rubio, and Claudio Verdozzi. Microscopic theory of light-induced ultrafast skyrmion excitation in transition metal films. *npj Computational Materials*, 8(1), 2022.

[12] Amalio Fernández-Pacheco, Elena Vedmedenko, Fanny Ummelen, Rhodri Mansell, Dorothée Petit, and Russell P. Cowburn. Symmetry-breaking interlayer dzyaloshinskii-moriya interactions in synthetic antiferromagnets. 2018.

[13] P. Ehrenfest. Bemerkung über die angenäherte gültigkeit der klassischen mechanik innerhalb der quantenmechanik. *Zeitschrift für Physik*, 45(7-8):455 – 457, 1927.

[14] Bo. Yang. Numerical studies of dynamical micromagnetics. 1997.

[15] Ph Depondt and F G Mertens. Spin dynamics simulations of two-dimensional clusters with heisenberg and dipole-dipole interactions. *Journal of physics. Condensed matter : an Institute of Physics journal*, 21(33):336005, 2009.

[16] Z.A. Anastassi and T.E. Simos. Numerical multistep methods for the efficient solution of quantum mechanics and related problems. *Physics Reports*, 482:1 – 240, 2009.

[17] M.J.D. Powell. On search directions for minimization algorithms. *Mathematical Programming*, 4(1):193–201 – 201, 1973.